Structures 68 (2024) 107246

Contents lists available at ScienceDirect

Structures

journal homepage: www.elsevier.com/locate/structures

Efficient finite element reliability analysis employing sequentially-updated surrogate model for fragility curve derivation

Seungjun Lee [a], Jaebeom Lee [b], Sungsik Yoon [c], Young-Joo Lee [a,*]

[a] Department of Civil, Urban, Earth, and Environmental Engineering, Ulsan National Institute of Science and Technology (UNIST), Ulsan, Republic of Korea
[b] Division of Physical Metrology, Korea Research Institute of Standards and Science (KRISS), Daejeon, Republic of Korea
[c] Department of Artificial Intelligence, Hannam University, Daejeon, Republic of Korea

ARTICLE INFO

Keywords:
Structural reliability analysis
Finite element reliability analysis
First-order reliability method
Fragility curve
Surrogate model
Computational cost

ABSTRACT

As the threat of natural disasters to structures intensifies, risk assessment of infrastructure has gained much importance. Fragility curves are essential tools in predicting disaster-related losses and making disaster mitigation decisions. In this paper, we propose a new method to efficiently derive accurate fragility curves for structures with high levels of nonlinearity or complexity, addressing the computational challenges of conventional finite element reliability analysis (FERA). To reduce the computational cost for calculating probability of failure in FERA, the proposed method utilizes the first-order reliability method (FORM). However, even with this approach, the computational cost of deriving the fragility curve may remain high; therefore, a surrogate model is used to further reduce costs. By training the surrogate model using the initial structural damage probabilities for a few hazard intensities, an optimal starting point can be calculated for the subsequent FORM analysis. During the fragility analysis, the surrogate model can be updated sequentially to increase the efficiency of FORM analysis continuously. In particular, the training process of the surrogate model requires no separate or additional finite element analysis because it is constructed using previous FERA results. The accuracy and efficiency of the proposed method are tested using conventional FERA and Monte Carlo simulations through a hypothetical short-column example. In addition, fragility curves are derived through a bridge flood fragility assessment considering the scour and seismic vulnerability assessment of a buried gas pipeline considering soil-structure interactions. The derived fragility curves closely match those derived using the conventional FERA, and the computational costs are reduced by 36.54 % and 52.38 %, respectively, compared with the conventional FERA, confirming its cost-effectiveness.

1. Introduction

Natural disasters such as floods and earthquakes can cause significant damage to structures, leading to casualties, property damage, and long-lasting economic and social impacts. Thus, disaster risk assessment and mitigation efforts have become increasingly important in the fields of engineering, urban planning, and disaster management [1,2]. Fragility curves are essential tools for predicting losses and in decision-making processes for disaster mitigation. For instance, risk assessment tools such as HAZUS-MH [3], ERGO-EQ [4], SYNER-G [5], and OpenQuake [6] have been developed to utilize fragility curves for assessing post-disaster losses under various scenarios. Thus, many studies have focused on accurately and efficiently deriving fragility curves for various structures subjected to natural disasters because predicting structural damage is crucial for disaster mitigation and decision-making [7–10].

Fragility curves are derived by estimating the probability of failure when structures exceed a pre-determined damage threshold, which varies depending on the hazard intensity measures (IMs) applicable to the type of natural disaster, considering the various uncertainties affecting the structural response. Examples of IMs widely used in earthquake scenarios are peak ground acceleration (PGA), peak ground velocity, and spectral acceleration [11]. Similarly, the IMs often used for flood events include water velocity, water depth, and duration of the flood [12]. Four major methods are often utilized to derive fragility curves: empirical, analytical, hybrid, and judgmental [13,14]. Empirical methods rely on the statistical analysis of historical damage data to develop fragility curves based on observed damage patterns [15,16]. In

* Corresponding author.
E-mail address: ylee@unist.ac.kr (Y.-J. Lee).

https://doi.org/10.1016/j.istruc.2024.107246
Received 28 February 2024; Received in revised form 23 July 2024; Accepted 4 September 2024
Available online 12 September 2024

contrast, analytical methods use the mathematical modeling of structures and natural hazards to derive fragility curves through theoretical calculations [17,18]. Hybrid methods properly integrate aspects of empirical and analytical methods [5,19]. Finally, in judgmental methods, experts provide their opinions on the likely damage states for specific structural types and natural hazards. To derive a fragility curve and utilize it appropriately to obtain accurate results, it is crucial to thoroughly understand the strengths and limitations inherent in each methodological approach.

Among the four abovementioned approaches, the analytical method offers the distinct advantage due to its objectivity, being unaffected by empirical data and subjective assessments. In this approach, finite element analysis (FEA) is often combined with reliability analysis to estimate the fragility curves [20]. Particularly when the structural non-linearity or complexity of the target structure is significant, reliability analysis can be carried out in conjunction with sophisticated FEA, commonly known as finite element reliability analysis (FERA) [21]. However, despite the high level of accuracy, deriving fragility curves using FERA can be computationally demanding because it requires iteratively calculating the probability of damage to a structure, considering various disaster scenarios such as earthquakes or floods. Although several researchers have adopted the first-order reliability method (FORM), which is a non-sampling-based method for structural reliability analysis, the computational cost to perform FERA more efficiently remains high.

In recent years, the advancement of artificial intelligence (AI) has offered novel approaches for the development of fragility curves across a variety of structures and natural disasters [10,22]. In this context, surrogate models play a crucial role by providing computationally efficient alternatives to complex physics-based models, such as finite element (FE) models [23]. A surrogate model, also known as a metamodel, is a simplified representation that approximates the behavior of these complex systems with significantly reduced computational requirements. These surrogate models often rely on comprehensive datasets, which encompass a wide range of system behaviors under various scenarios, include relevant input features that impact outputs, and provide a clear understanding of the underlying physical processes. Specifically, the process of developing a surrogate model involves training it with a dataset that contains both the input parameters (e.g., structural properties) and the corresponding outputs (e.g., structural responses) from complex physics-based models (e.g., FE models). Once trained, a surrogate model can predict outputs for new input values, significantly reducing computational costs compared to running the complex model every time. Therefore, due to its several advantages, the application of surrogate models to derive fragility curves has become increasingly popular, offering a cost-effective method that utilizes analytical approaches.

For example, Ghosh et al. [24] proposed surrogate models to effectively capture the seismic behavior of bridge components and to estimate corresponding fragility curves. They have shown how surrogate models can significantly enhance computational efficiency when predicting the seismic activity of bridge components, as compared to traditional Monte Carlo simulation (MCS) methods. Similarly, Zhang and Wu [25] proposed a kriging model-based approach to establish seismic fragility curves for reinforced concrete (RC) bridges with reduced computational effort. Kim et al. [26] developed a deep neural network (DNN) based probabilistic model to assess the seismic responses of structural systems and to derive fragility curves of RC frame structures. Khandel and Soliman [27] suggested a probabilistic framework for assessing the fragility of bridges subjected to flooding and flood-induced scour using two DNNs. Surrogate models also enable efficient fragility analysis under multi-hazard scenarios [28,29]. Additionally, meta-databases of structures have been developed to further facilitate these analyses [30]. For the task of structural fragility analysis, these surrogate model-based methods offer considerable computational efficiency and accuracy in predicting the seismic and flood-induced responses of target structures. However, despite their advantages, surrogate models have several limitations [31]. They might lead to errors or inaccuracies in estimating the relationships between predictor variables and their predicted responses, and the selection of sample points and calibration of the surrogate model can be challenging. In addition, surrogate models may be unable to capture complex or rare events outside the range of a training dataset, and generating an appropriate training dataset may be expensive and time-consuming.

The paper proposes a novel analytical method to address the limitations identified in previous studies for the effective estimation of fragility curves. The proposed method utilizes the FORM to reduce the cost of FERA and introduces a sequentially updated surrogate model to further minimize the computational costs. As the probabilities of structural damage are initially assessed for selected IM values, the surrogate model is trained to predict structural responses using data from previous FERA outcomes. Subsequently, for the following FORM analysis, the surrogate model can offer an optimized starting point. The surrogate model can be sequentially refined as the fragility analysis progresses; thus, continuously improving the computational efficiency for the FORM analyses that follow. Notably, the method enhances computational efficiency without necessitating additional FEA for training the surrogate model, as it is constructed exclusively from previous FERA results. The application of this method is detailed further in the subsequent sections, focusing on sophisticated FEA-based fragility curve derivation.

2. Proposed method

2.1. FERA employing computational platform

The concept of a fragility curve is defined by the association between hazard intensity metrics and the probability of structural failure once thresholds are surpassed. The calculation of failure probability can be achieved via simulations or analytical methods, which are typically categorized into sampling-based and analytical function-based methodologies [21]. Sampling-based methods such as MCS are theoretically simple. The probability of failure is estimated by conducting a sequence of numerical simulations and counting the number of failure events among all simulated events [32]. With sufficient samples, MCS can provide accurate results, regardless of the structural analysis technique. However, the computational cost of sampling-based methods can increase significantly, particularly when the structural analysis itself is expensive or the probability of failure is low, requiring many structural analyses. On the other hand, analytical function-based methods express the failure probability as the conditional probability of reaching a pre-determined limit state at a specific level of hazard intensity. In this approach, the limit-state function is defined as an algebraic function of random variables (RVs), which represents the discrepancy between structural capacity and demand. However, the application of function-based analytical methods is often confined to simpler structures due to their limitations; thus, the responses of highly complex structural systems cannot be expressed explicitly.

This paper addresses the challenge of computational complexity by employing FERA, which integrates a sophisticated FE model, and FORM, a non-sampling method often used for reliability analysis because of its computational efficiency. In FORM analysis, the failure probability associated with a specific limit-state function, represented as $g(\mathbf{x})$, can be computed by defining an event (i.e., failure) with selected RVs. The limit-state of failure is then formulated as a function of the original space variables, denoted by $\mathbf{x}$, where $\mathbf{x}$ is the column vector representing the RVs. These RVs, in their original space, are converted to a standard normal space through a one-to-one mapping transformation matrix. Following this transformation, the function that defines the limit state, now expressed as $G(\mathbf{u})$, is described in terms of $\mathbf{u}$, where $\mathbf{u}$ represents the vector of standard normal variables. To obtain the failure probability using FORM, we solve a geometric optimization problem using the limit-

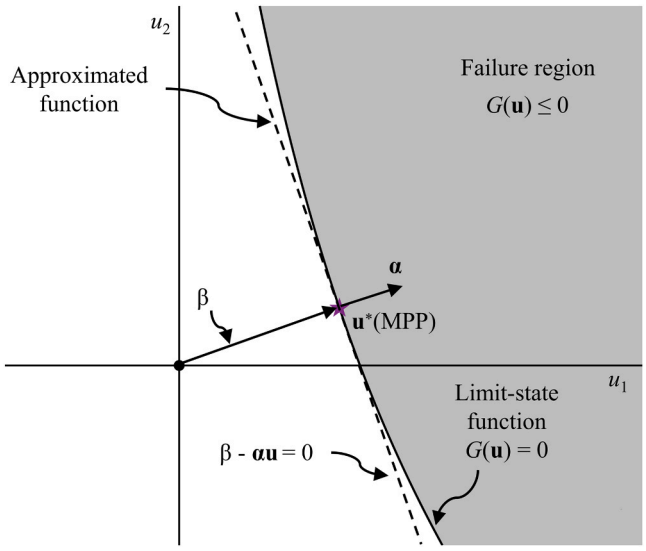

Fig. 1. Linear approximation in FORM.

state function converted to a standard normal space as follows:

$$\mathbf{u}^* = \arg\min\{\|\mathbf{u}\| | G(\mathbf{u}) = 0\} \tag{1}$$

where "arg min" represents the argument of the minimum of a function, and $||\cdot||$ denotes the L^2-norm. The point $\mathbf{u}^*$ lies on the surface defined by the limit-state function $G(\mathbf{u}) = 0$ and is acknowledged as the most likely point, also known as the *most probable point* (MPP), which has the maximal probability of occurrence within the failure domain where $G(\mathbf{u})$ is less than or equal to zero. The definition of failure represented by the limit-state function can be subsequently estimated by employing a first-order Taylor series expansion as follows:

$$G(\mathbf{u}) \cong \nabla G(\mathbf{u}^*)(\mathbf{u} - \mathbf{u}^*) = \|\nabla G(\mathbf{u}^*)\|(\beta - \alpha\mathbf{u}) \tag{2}$$

where $\nabla G(\mathbf{u})$ is the gradient vector, α is the normalized negative gradient vector at the MPP, expressed as $-\nabla G(\mathbf{u}^*)/||\nabla G(\mathbf{u}^*)||$, and β represents the reliability index, determined as the minimum distance from the origin to the approximated limit-state function within the domain of the standard normal space. The probability of failure, denoted P_f, is then derived as follows:

$$P_f = \Phi(-\beta) \tag{3}$$

where $\Phi(\cdot)$ is the cumulative distribution function associated with the standard normal distribution. The linearized limit-state function for a two-dimensional standard normal space within the failure domain is depicted in Fig. 1. Through the process of linearizing the failure surface, FORM analysis facilitates a cost-effective approach to estimating the failure probability. For additional information on the FORM, interested readers can refer to references [33,34].

To perform FERA efficiently, this paper introduces a computational platform. Several FERA platforms have been devised and utilized for a variety of structural integrity and vulnerability evaluations. For instance, Lee et al. [35] proposed Finite Element Reliability Using MATLAB (FERUM)-ABAQUS for analyzing the component and system reliability of the torque box of an aircraft wing. Lee and Moon [21] developed FERUM-ZEUS, a tool for assessing the seismic vulnerability of three-dimensional building structures. Additionally, a Python-based interface for FERUM and ABAQUS, known as PIFA, has been introduced by Lee et al. [36] for deriving flood fragility curves. These platforms are integrated with two software packages, maximizing their individual advantages to address the complex and diverse structural reliability problems effectively. In this paper, we introduce PIFA for efficiently estimating fragility curves and present the typical data flow representation in PIFA, as shown in Fig. 2.

Fig. 2 illustrates the computational platform, which includes three components: (1) FERUM for conducting reliability analysis, (2) ABAQUS for performing FEA, and (3) PIFA as the interface bridging the two software packages. Developed by researchers at the University of California, Berkeley [37], FERUM is an open-source MATLAB package that supports various reliability analysis methodologies, such as FORM. ABAQUS is a widely used commercial software package for FEA. Within this integrated platform, PIFA has been strategically designed to manage the FERA process efficiently by interacting with FERUM and ABAQUS. FERUM iteratively offers deterministic input values of RVs to PIFA, which facilitates the construction of FE models with variable inputs and their subsequent transmission to ABAQUS. Following this, ABAQUS performs FEA and conveys the required structural responses, such as stress, strain, and displacement, back to FERUM through PIFA. In the FERA process using FORM, an optimization problem such as Eq. (1) is solved numerically to obtain intermediate results. Therefore, in the proposed method, a surrogate model is iteratively refined using the outcomes from previous FORM analyses. The following section provides a detailed description of the surrogate model construction.

2.2. Surrogate model construction using Gaussian process regression

A common approach for solving time-consuming physics-based models (i.e., FE models) in the field of structural reliability is to employ deterministic computations for the estimation of surrogate model parameters [38]. This process enables the use of commercial FEA software for calculating structural responses directly, without implementing the need for the stochastic FE model formulations that alternative methods require [39]. Several surrogate models are available, including first- and second-order polynomial regression models, which have been widely used because of their efficiency in structural reliability problems (i.e., response surface approaches) [40]. More recently, researchers have explored alternative approaches, such as artificial neural networks [41], support vector machines [42], and Kriging interpolation models, also referred to as Gaussian process regression (GPR) [43–45]. This paper focuses on GPR, which, although more sophisticated than polynomial regression models, offers advantages such as high-accuracy interpolation of complex functions and a localized measure of uncertainty for model predictions.

GPR is a machine learning-based approach that constructs a flexible

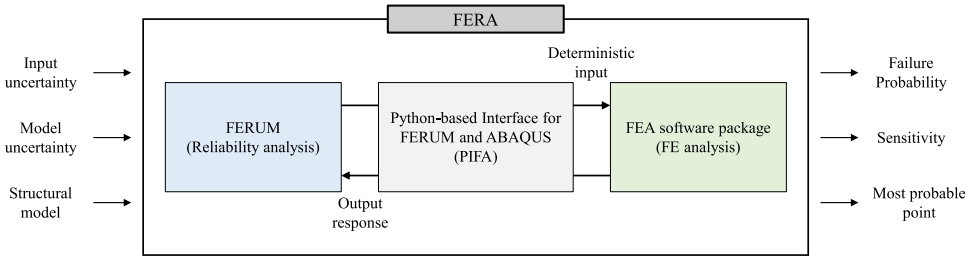

Fig. 2. Illustration of a typical data flow in PIFA.

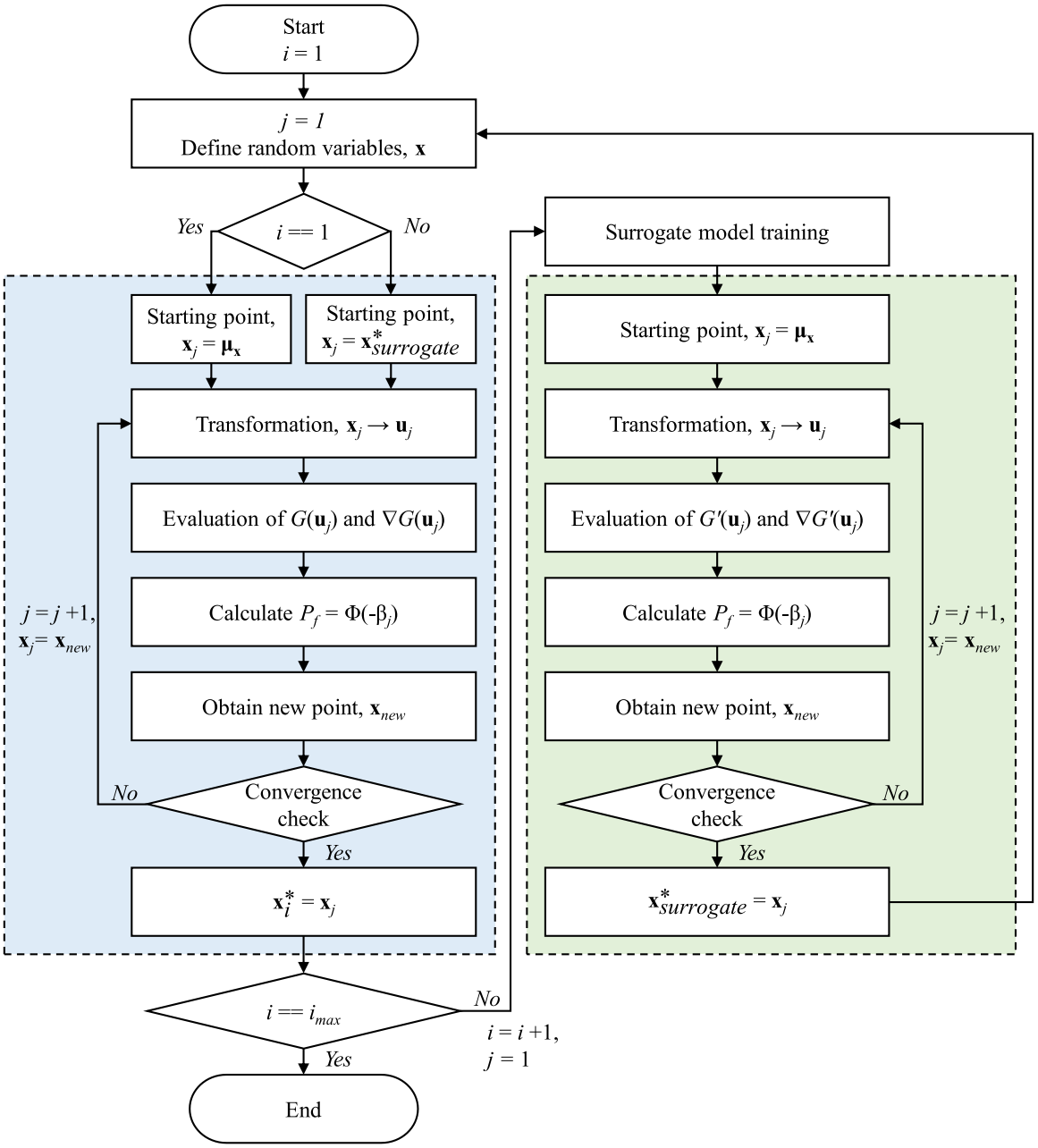

Fig. 3. Flow chart of the proposed method for fragility curve derivation.

Bayesian model to predict outcomes with probabilities [46]. It assumes that all data points are multivariate and normally distributed, suggesting that any subset of the multivariate dataset will also follow a Gaussian distribution. In this paper, we define the data matrix (**D**), which contains the FEA results, RVs, and hazard IM values previously analyzed by FORM, as shown below:

$$\mathbf{D} = \{(\mathbf{X},\ \mathbf{y})\} = \left\{\left(x_{ij},\ y_i\right) \middle| i = 1,\ \ldots, N_{FE}; j = 1,\ \ldots, N_{RV} + N_{IM}\right\} \tag{4}$$

where **X** and **y** constitute the matrix for the input RVs and hazard IM values, and the output vector of the FEA results, respectively. N_{FE} denotes the count of FEAs, N_{RV} denotes the number of RVs, N_{IM} denotes the number of IMs. The element x_{ij} represents the input for the i^{th} FEA and j^{th} input variable (i.e., RV or IM value), while y_i corresponds to the related FEA outcome. Thus, the function $\widehat{f}_*(\cdot)$ can be defined for any new input matrix of $\mathbf{X}_*$ by applying the multivariate normality, which is the Gaussian process (GP) assumption:

$$\begin{pmatrix} \mathbf{y} \\ \widehat{f}_*(\mathbf{X}_*,\ \widehat{\boldsymbol{\theta}}) \end{pmatrix} = N\left(\mathbf{O},\ \boldsymbol{\Sigma}\right) = N\left(\mathbf{O},\ \begin{bmatrix} \mathbf{K} + \sigma^2_{noise}\mathbf{I} & \mathbf{K}_* \\ \mathbf{K}_*^{\mathrm{T}} & \mathbf{K}_{**} \end{bmatrix}\right) \tag{5}$$

where $\widehat{\boldsymbol{\theta}}$ represents vector of the hyperparameters that have been optimized. The multivariate Gaussian distribution is denoted by N. The covariance matrix, denoted by $\boldsymbol{\Sigma}$, is positive semi-definite and symmetric, and **O** represents the zero matrix. The covariance matrix for the input x_{ij}, denoted **K**, describes the variance within inputs, while $\mathbf{K}_*$ is the matrix that expresses the covariances between the known inputs **X** and the new prediction inputs $\mathbf{X}_*$. Additionally, $\mathbf{K}_{**}$ represents the covariance within the new prediction input $\mathbf{X}_*$, and σ^2_{noise} is indicative of the noise variance. The development of the covariance matrix (i.e., **K**, $\mathbf{K}_*$, and $\mathbf{K}_{**}$) in GPR typically involves a kernel function predicated on the Euclidean distance between any two vectors $\mathbf{z}$ and $\mathbf{z}'$. Specifically, the covariance matrices are formulated using a kernel function considering the standard deviations (i.e., $\sigma_{\mathbf{z}}$ and $\sigma_{\mathbf{z}'}$), and the correlation coefficient

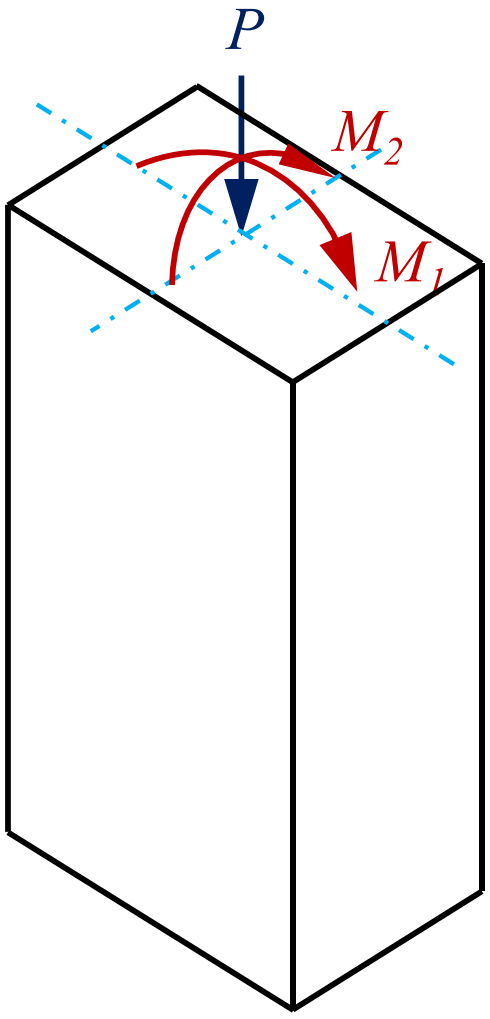

Fig. 4. Short column subjected to axial force and biaxial bending moments.

($\rho_{\mathbf{zz}'}$) between the vectors $\mathbf{z}$ and $\mathbf{z}'$:

$$k(\mathbf{z},\ \mathbf{z}') = \sigma_{\mathbf{z}}\sigma_{\mathbf{z}'}\rho_{\mathbf{zz}'} \tag{6}$$

This paper introduces a squared exponential kernel with two hyperparameters for the formulation of the covariance matrix [47]:

$$k_{SE}\left(\mathbf{z},\ \mathbf{z}'\right) = \theta_1^2 \exp\left(-\frac{\|\mathbf{z}-\mathbf{z}'\|^2}{2\theta_2^2}\right) \tag{7}$$

where θ_1 is the variance hyperparameter governing the function's vertical fluctuation, and θ_2 dictates the horizontal length-scale of the function. To achieve a surrogate model of high accuracy, it is essential to finely tune these hyperparameters; a task often accomplished using maximum likelihood estimation within GPR. A multivariate normal distribution can be used to define the conditional probability of given dataset (i.e., $\mathbf{X}$ and $\mathbf{y}$) specified by Eq. (5):

$$p\left(\mathbf{y}|\mathbf{X}\right) = \frac{1}{(2\pi)^{N_{FE}/2}|\mathbf{\Sigma}|^{1/2}} \exp\left(-\frac{1}{2}\mathbf{y}^{\mathrm{T}}\mathbf{\Sigma}^{-1}\mathbf{y}\right) \tag{8}$$

Eq. (8), which is represented as a conditional probability, can be expressed by taking the natural logarithm for computational convenience:

$$\begin{aligned}\mathscr{L}(\boldsymbol{\theta}|\mathbf{X}) &= -\ln p(\mathbf{y}|\mathbf{X}) \\ &= \frac{N_{FE}}{2}\ln\left(2\pi\right) + \frac{1}{2}\mathbf{y}^{\mathrm{T}}\left(\mathbf{K}+\sigma_{noise}^2\mathbf{I}\right)^{-1}\mathbf{y} + \frac{1}{2}\ln\left|\mathbf{K}+\sigma_{noise}^2\mathbf{I}\right|\end{aligned} \tag{9}$$

where the negative log-likelihood function is denoted by $\mathscr{L}(\cdot)$. We subsequently minimize $\mathscr{L}(\cdot)$ to obtain the optimized hyperparameter $\widehat{\boldsymbol{\theta}}$:

$$\widehat{\boldsymbol{\theta}} = \arg\min_{\boldsymbol{\theta}}(\mathscr{L}) \tag{10}$$

For more information on GPR, including kernel functions, see references [45,47].

2.3. Sequentially-updated surrogate model for FERA

Although the FORM has been introduced in fragility curve derivation, it incurs a high computational cost. Therefore, this paper employs GPR as a surrogate model, which is detailed in Section 2.2, to address this problem. Initially, the proposed method utilizes FERA to estimate the structural damage probability at the initial hazard IM value, and then captures the structural responses depending on different RV input values within the optimization loop of FORM analysis. Based on the FERA outcomes, a surrogate model is trained. Subsequently, a preliminary FORM analysis, employing this surrogate model, is conducted for the next IM value. This approach establishes an optimized starting point for the ensuing FORM analysis within FERA. The primary FERA analysis continues from this optimally determined point. The primary analysis using FERA then proceeds from this strategically determined point. Fig. 3 provides a flow chart representation of the proposed method.

The procedure of the proposed method is summarized as follows (see Fig. 3 for the flowchart):

1. Initialization and definition of variables: The intensity index i is initialized at 1, and $i_{\max}$ represents the total number of IM values considered for deriving the analytical fragility curve. The RVs that serve as inputs to the FERA are defined, where j indicates the index of the inner loop of the FORM analysis. This index j is used to manage iterations within each level of intensity (i.e., the i^{th} level), allowing for the FORM analysis of each scenario.
2. FORM analysis starting points: If the intensity index i is 1, the FORM analysis in FERA begins at the mean values ($\boldsymbol{\mu}_{\mathbf{x}}$) of RVs, which correspond to the origin in the standard normal space, same as conventional FORM analysis. For subsequent indices (i.e., $i > 1$), the analysis begins at the optimal starting point ($\mathbf{x}^*_{surrogate}$) provided by a surrogate model.
3. FORM analysis execution with FE model (i.e., FERA): The transformation of variables $\mathbf{x} \rightarrow \mathbf{u}$ is performed [48]. The functions $G(\mathbf{u})$ and $\nabla G(\mathbf{u})$ are evaluated using the FE model. The probability of failure P_f is calculated based on the reliability index β, as specified in Eq. (1).
4. Iteration and convergence check: A new point $\mathbf{x}_{new}$ is obtained, and a convergence of each iteration is checked as follows:

$$|G(\mathbf{u})| \le \varepsilon_1 \text{ and} \left\|\mathbf{u} - \boldsymbol{\alpha}^{\mathrm{T}}\mathbf{u}\boldsymbol{\alpha}\right\| \le \varepsilon_2 \tag{11}$$

   where the threshold values are defined as $\varepsilon_1 = 0.01$ and $\varepsilon_2 = 0.05$ in this study. If the convergence criteria are met (i.e., Eq. (11)), the analysis updates $\mathbf{x}_j$ to the current MPP ($\mathbf{x}_i^*$). If not, the analysis continues by considering $\mathbf{x}_{new}$ in the next iteration within the same intensity index. The process is repeated until convergence is achieved, after which j is reset to 1 and i is incremented if i has not yet reached i_{max}.
5. Surrogate model training and application: After estimating the P_f and MPP values that satisfy the convergence criteria, and if i has not yet reached i_{max}, a GPR-based surrogate model is constructed. This surrogate model utilizes input-output pairs from the previous FORM analysis in FERA, along with the corresponding intensity measure values, as described in Section 2.2. Subsequently, the surrogate model is employed to perform the conventional FORM analysis for

Table 1
Statistical properties of RVs for the short column example.

RV	Distribution type	Mean	COV	Correlation Coefficient			
				M_1	M_2	P	σ_y
M_1 (kN·m)	Normal	250	0.3	1.0			sym.
M_2 (kN·m)	Normal	125	0.3	0.5	1.0		
P (kN)	Log-Normal	2000 to 3000	0.2	0.3	0.3	1.0	
σ_y (MPa)	Log-Normal	40	0.1	0	0	0	1.0

the next intensity index. Notably, the functions $G'(\mathbf{u})$ and $\nabla G'(\mathbf{u})$ are calculated using the surrogate model. Furthermore, the surrogate model identifies the optimized starting point ($\mathbf{x}^*_{surrogate}$) for the next intensity level, which is then utilized as the starting point for the next iteration within the FERA loop.

6. Loop continuation and fragility curve derivation: These optimal points are utilized as starting points for the FERA loop as it continues. Once the intensity index finally reaches i_{max}, an analytical fragility curve is derived.

In Fig. 3, the light blue dashed box on the left describes the FORM analysis conducted using the FE model. On the other hand, the light green dashed box on the right indicates FORM analysis performed using the surrogate model. Specifically, the input-output pairs used for training the surrogate model are exclusively derived from the values obtained within the light blue dashed box.

The proposed method enables sequential updates of the surrogate model as the FERA progresses, continuously resulting in enhanced efficiency of the FORM-based FERA. An important advantage of this approach is that no additional FEA computations are needed in the training process of surrogate model; instead, it can be entirely based on the data derived from prior FERA results. The following Sections demonstrate the effectiveness of the proposed method with several examples, including the number of FEA iterations, accuracy of the analysis results, comparison with conventional methods, and computational cost.

3. Illustrative example: short column subjected to axial force and biaxial bending moments

An illustrative example is introduced to demonstrate the effectiveness and advantages of the proposed method. The proposed method is applied to a simple hypothetical example of a short column [34] that is subjected to both an axial force P, and biaxial bending moments, M_1 and M_2, as depicted in Fig. 4. The column material property is assumed to be elastic and perfectly plastic with a yield strength σ_y, and the failure of the column is expressed by the following limit-state function:

$$g(\mathbf{x}) = 1 - \frac{M_1}{S_1\sigma_y} - \frac{M_2}{S_2\sigma_y} - \left(\frac{P}{A\sigma_y}\right)^{\theta} \tag{12}$$

where $\mathbf{x} = [M_1, M_2, P, \sigma_y]^T$ represents the vector of RVs, $\theta = 2$ is a parameter associated with the limit-state function, $A = 0.190\ \text{m}^2$ is the cross-sectional area, and $S_1 = 0.030\ \text{m}^3$ and $S_2 = 0.015\ \text{m}^3$ are the flexural moduli of the fully plastic column section in two directions. The statistical properties of these variables are detailed in Table 1, which includes the distribution type, mean, coefficient of variation (COV), and correlation coefficients for the RVs.

The analysis is performed by increasing the axial force from 2000 to 3000 kN at intervals of 50 kN, considering the axial force as an IM. In this illustrative example, the starting point at an intensity index of 1 (i.e., $P = 2000$ kN) is $[250, 125, 2000, 40]^T$, based on the RVs listed in Table 1. The FORM analysis is then conducted as indicated by the light blue dashed box in Fig. 3. After several iterations in the FORM analysis loop, convergence is achieved, and we obtain the reliability index and MPP of $\beta = 3.122$ and $\mathbf{x}^*_1 = [401.436, 200.718, 2820.923, 33.368]^T$, respectively. A total of 30 structural analyses (i.e., G-function evaluations) are performed at this intensity index. Next, a surrogate model needs to be constructed because the intensity index has not yet reached its maximum value (i.e., 21 in this example). The surrogate model is constructed based on the results of the previous FORM analysis using the structural analysis model. Utilizing this trained surrogate model, the FORM analysis is conducted for the next intensity level (i.e., $P = 2050$ kN) as indicated by the light green dashed box in Fig. 3, and $\mathbf{x}^*_{surrogate}$ is calculated as $[398.322, 199.137, 2889.922, 33.466]^T$. Subsequently, as depicted in Fig. 3, the FORM analysis with the structural analysis model is conducted for $P = 2050$ kN. The starting point for this

Table 2
Comparison of results of MCS, conventional FERA, and proposed method for the short column example.

Intensity index	IM	MCS (COV ≤ 0.05)		Conventional FERA		Proposed method	
No.	Axial force (P)	Reliabilityindex (β)	G-fun. counts	Reliabilityindex (β)	G-fun. counts	Reliabilityindex (β)	G-fun. counts
1	2000	3.110	426,827	3.122	30	3.122	30
2	2050	3.059	359,619	3.074	30	3.075	5
3	2100	3.002	298,270	3.027	30	3.027	5
4	2150	2.976	273,801	2.979	30	2.979	5
5	2200	2.906	218,346	2.931	24	2.931	5
6	2250	2.865	191,513	2.883	24	2.883	5
7	2300	2.819	166,064	2.835	24	2.835	5
8	2350	2.786	149,372	2.786	24	2.786	5
9	2400	2.734	127,709	2.738	24	2.738	5
10	2450	2.672	105,679	2.689	24	2.689	5
11	2500	2.618	90,091	2.641	24	2.641	5
12	2550	2.571	78,485	2.593	24	2.593	5
13	2600	2.526	68,889	2.545	24	2.545	5
14	2650	2.482	60,969	2.497	24	2.497	5
15	2700	2.423	51,592	2.449	24	2.449	5
16	2750	2.377	45,456	2.401	24	2.401	5
17	2800	2.330	40,088	2.354	24	2.354	5
18	2850	2.312	38,073	2.307	24	2.306	5
19	2900	2.248	32,232	2.260	24	2.260	5
20	2950	2.195	28,073	2.213	24	2.213	5
21	3000	2.164	25,855	2.167	24	2.166	5
Total	-	-	2,877,003	-	528	-	130

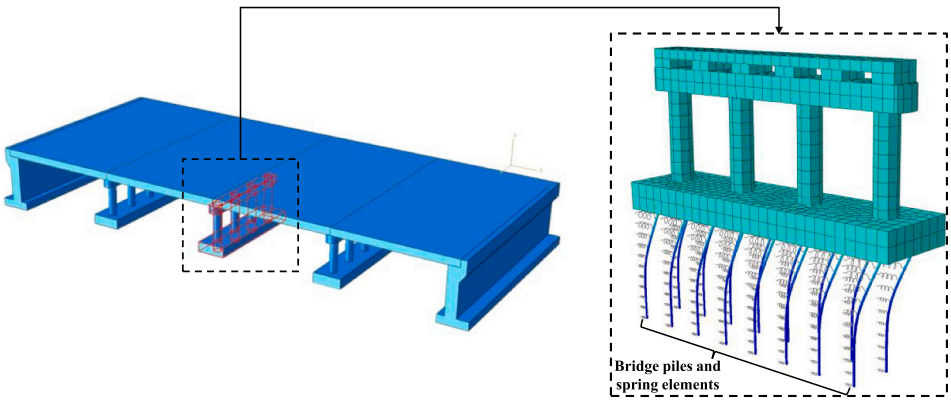

Fig. 5. FE model for bridge structure and bridge pier.

Table 3
Statistical properties of RVs for flood fragility assessment.

RV	Distribution type	Mean	COV
Concrete mass density (kg/m^3)	Normal	2300	0.3
Steel bar mass density (kg/m^3)	Normal	7861.5	0.3
Pile steel mass density (kg/m^3)	Normal	7868.6	0.2
Water pressure intensity scale factor	Normal	1.0	0.1

Table 4
Damage states and corresponding ductility demands.

Damage state	Ductility demand
Minor damage (First plastic hinge occurrence)	$1.0 \leq D_d \leq 3.3$
Major damage (Second plastic hinge occurrence)	$3.3 < D_d \leq 7.0$
Collapse	$D_d > 7.0$

analysis is $\mathbf{x}^*_{surrogate}$, and a total of 5 structural analyses are required. This process will continue in a loop, repeating until the intensity index reaches its maximum value of 21, at which point the procedure will terminate.

The effectiveness is tested by comparing the proposed method with MCS and conventional FERA methods. The results of the analysis, including the reliability index and the count of limit-state function evaluations for each method are presented in Table 2. It is important to note that with regard to MCS, 2,877,003 limit-state function evaluations have been conducted, indicating that a considerable sample size is necessary for the structural reliability analysis. The minimum number of samples required for the MCS depends on the probability of failure, which increases exponentially as the probability of failure decreases. Therefore, when the FEA is time-consuming, depending on the type of analysis and FE model, the sampling-based FERA may be limited. As illustrated in Table 2 and Fig. 3, the proposed method corresponds to the conventional FERA when the intensity index is 1, yielding identical reliability indices and numbers of limit-state function evaluations. However, when the intensity index is 2 or greater, a surrogate model is constructed and sequentially updated to provide an optimal starting point, thereby significantly reducing the number of limit-state function counts. This confirms that the proposed method can calculate the failure probability with nearly the same accuracy as the conventional FERA, but at a much lower computational cost of approximately 25 %.

4. Application example I: flood fragility of bridge considering scour

4.1. Problem description

To describe the benefits of the proposed method for deriving fragility curves, we select an application example using FERA. Lee et al. [36] conducted fragility analyses of a bridge using FERA, considering water velocity as an IM to construct fragility curves and explained the accumulation of debris and the corrosion effect. The same bridge structure is used in this paper. The bridge structure discussed by Lee et al. [36] was an RC bridge 30 m wide and 63 m long and consisted of a slab, abutment, pier, and mass concrete between the slab and piers. The bridge design followed the Korea Highway Bridge Design Specification (KHBDS) [49] which has the following four key features:

- Strength-based design: This specification adopts a strength design approach, emphasizing structural safety by ensuring structural capacities meet or exceed expected design loads with serval factors.
- Load calculations: The specification encompasses a comprehensive array of design load combinations, including dead loads, live loads with standardized truck configurations, seismic loads with specified design return periods, and wind loads.
- Material properties: It details specific material properties required for bridge design, such as concrete's compressive strength and steel's yield strength.
- Structural configurations: The KHBDS contains the design and layout of various bridge components, including girders, piers, and structural types such as steel, concrete, composite, and truss bridges commonly used in highway bridge design.

As shown in Fig. 5, the ABAQUS FE model of the bridge was developed based on the original design specifications. A specific group of piers, which were identified as having the maximum stress and displacement, was selected for a preliminary analysis to enhance computational efficiency. This group of piers consists of a top concrete layer, multiple RC piers, and a foundational concrete base. Further details on the dimensions and material specifications of the pier structure are provided in [36].

In this paper, the flood fragility assessment incorporates the approach suggested by Kim et al. [50], which considers the impact of bridge scour. Scour has a significant influence on the stability of bridge structures during flooding events, it should be appropriately considered in FE modeling for realistic flood fragility analysis. In the FE modeling framework for scour, variable scour depths are applied to each bridge pier. The soil is modeled as horizontal spring elements affixed to the bridge piers to establish fixed boundary conditions, as depicted in Fig. 5. When scour action results in soil removal, the stiffness values of these

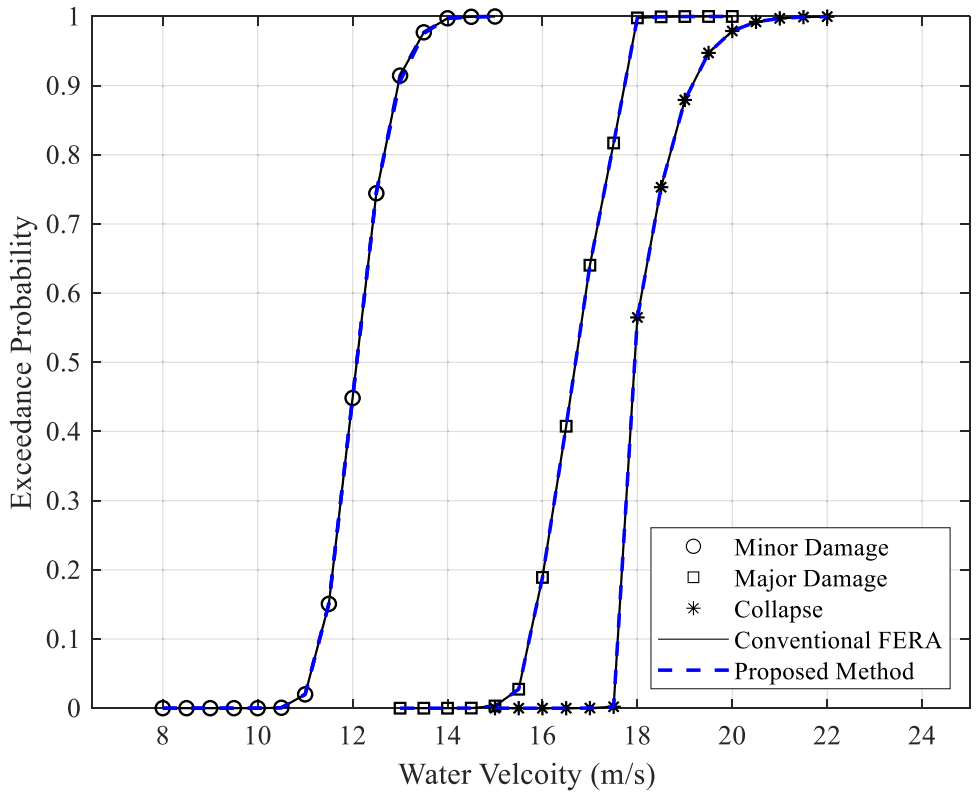

Fig. 6. Comparison of flood fragilities of the conventional FERA and proposed method according to damage state.

Table 5
Comparison of the computational cost of the conventional FERA and proposed method according to damage state.

Damage state	Number of FEAs		Efficiency
	Conventional FERA	Proposed method	
Minor damage ($8 \leq$ Water velocity (m/s) ≤ 15)	392	226	42.35 %
Major damage ($13 \leq$ Water velocity (m/s) ≤ 20)	348	220	36.78 %
Collapse ($15 \leq$ Water velocity (m/s) ≤ 22)	319	226	29.15 %
Total	1059	672	36.54 %

Table 6
Material properties of API 5L X65 gas pipeline.

Yield strength (MPa)	Elastic modulus (GPa)	Poisson's ratio	Mass density (kg/m^3)	Thickness (mm)	Coefficient of friction
445	210.7	0.3	7850	17.5	0.8

spring elements are minimized to reflect the loss of structural support. An expanded description of the methodology for bridge scour, which includes scour depth calculations for both a single pier and multiple piles, can be found in [50].

In this application example, the mass density and water pressure intensity are considered as RVs to account for the material property uncertainty, bridge self-weight uncertainty, and water pressure uncertainty, respectively. Additionally, the water pressure is multiplied by the water pressure intensity scale factor to consider the uncertainty in the water pressure caused by the water velocity. The RVs are assumed to be statistically independent, and their statistical properties, including the probability distribution type, mean, and COV, are determined based on references [51,52] and are summarized in Table 3.

In the fragility analysis, the limit states that consider the relevant failure modes of the bridge should be defined. This paper focuses specifically on addressing the lack of displacement ductility in bridge piles, which is a significant failure mode [50]. As detailed in Table 4 and based on references [53,54], the limit states are categorized into three distinct levels of damage: minor, major, and collapse. These damage states are characterized by the demand for displacement ductility (D_d), which is determined by the ratio of the resulting post-yield deformation, as following equation [55]:

$$D_d = \frac{\Delta_D}{\Delta_Y} \tag{13}$$

where Δ_D denotes the maximum displacement, and Δ_Y denotes the displacement at the yielding point of the bridge pile, respectively. The initial two damage states correspond to the occurrence of the first and second plastic hinges and are based on the structural responses observed.

4.2. Analysis result: flood fragility curves

A fragility analysis of the example bridge subjected to floods is performed using the proposed method and conventional FERA, and the results are presented in Fig. 6, based on the displacement ductility demands specified in Table 4. Flood fragility curves with three damage states are derived, and we observe that the probability of exceedance generally increases with increasing water velocity owing to deeper scour holes and stronger water pressure [50]. In addition, the fragility curves estimated using the conventional FERA and the proposed method are nearly identical.

Table 5 lists the number of FEAs and efficiency of the proposed method according to each damage state. For the conventional FERA, 392, 348, and 319 FEAs are required for minor damage, major damage,

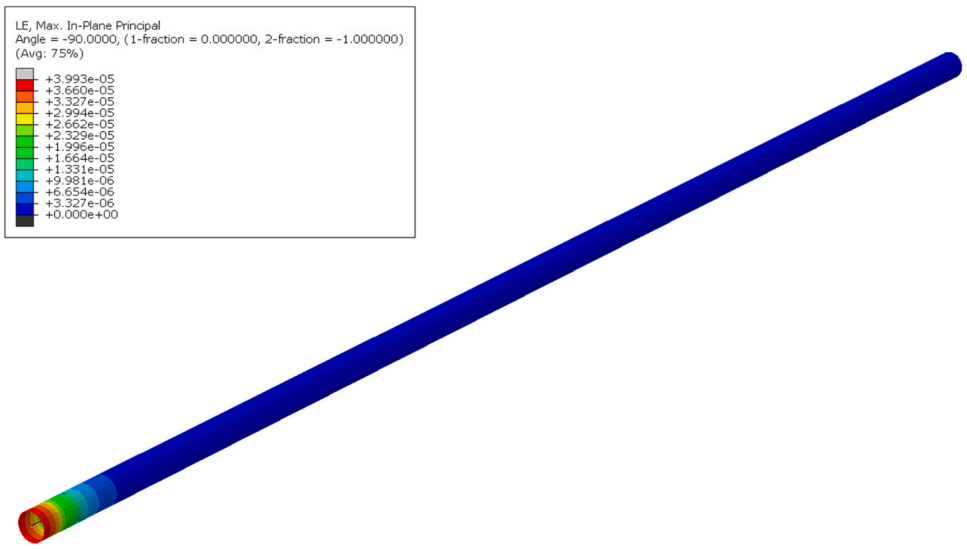

Fig. 7. FEA results of strain distribution for a buried gas pipeline.

Table 7
Selected input ground motions.

	Earthquake (Year)	Station	Mechanism	Magnitude	PGA (g)
EQ1	Gulf of Aqaba (1995)	Eliat	Strike slip	7.20	0.109
EQ2	Borrego (1968)	El Centro Array #9	Strike slip	6.63	0.130
EQ3	Cape Mendocino (1992)	Eureka-Myrtle & West	Reverse	7.01	0.178
EQ4	Chi-Chi (1999)	CHY014	Reverse Oblique	7.62	0.263
EQ5	Chi-Chi (1999)	ILA067	Reverse Oblique	7.62	0.198
EQ6	Coalinga−01 (1983)	Parkfield Fault Zone 1	Reverse	6.36	0.194
EQ7	Imperial Valley (1979)	Delta	Strike slip	6.53	0.351
EQ8	Kocaeli (1999)	Fatih	Strike slip	7.51	0.187
EQ9	Landers (1992)	Indio-Coachella Canal	Strike slip	7.28	0.109
EQ10	Loma Prieta (1989)	Hayward-BART	Reverse Oblique	6.93	0.159
EQ11	San Fernando (1971)	Whittier Narrows Dam	Reverse	6.61	0.107
EQ12	Tabas (1978)	Ferdows	Reverse	7.35	0.108

Table 8
Statistical properties of RVs for seismic fragility assessment.

RV	Distribution type	Mean	COV	Correlation coefficient			
				φ	c	γ	σ_y
φ (°)	Normal	38	0.10	1.0			sym.
c (kPa)	Normal	5	0.10	−0.7	1.0		
γ (kN/m^3)	Normal	18	0.10	0.3	0	1.0	
σ_y (MPa)	Log-Normal	467	0.07	0	0	0	1.0

and collapse, respectively, and a total of 1059 structural analyses are necessary to derive three fragility curves. In contrast, the proposed method requires 226, 220, and 226 FEAs for each damage state and 672 structural analyses. Therefore, the efficiency of the proposed method is calculated as

Table 9
Damage states and corresponding structural responses.

Damage state	Structural response
Minor damage (Minor leakage)	$\varepsilon_p \leq 0.7\varepsilon_y$
Moderate damage (Partial leakage)	$0.7\varepsilon_y < \varepsilon_p \leq \varepsilon_y$
Major damage (Complete rupture)	$\varepsilon_p > \varepsilon_y$

$$\text{Efficiency} = \left(1 - \frac{\text{the number of FEA of the proposed method}}{\text{the number of FEA of conventional FERA}}\right) \times 100 \tag{14}$$

Thus, the proposed method improves the efficiency of computational cost by approximately 36.54 %. This confirms that the proposed method can derive a flood fragility curve cost-effectively.

5. Application example II: seismic fragility of buried gas pipeline considering soil-structure interaction

5.1. Problem description

The proposed method is applied to a seismic fragility analysis that involves a nonlinear time-history analysis with a number of earthquake ground motions. Yoon et al. [56] performed a seismic fragility analysis of a buried gas pipeline by accounting for the uncertainty of soil parameters, through nonlinear time-history analyses using 12 selected earthquake ground motions. In addition, a beam on a nonlinear Winkler foundation (BNWF) model [57] was utilized to represent the soil-pipeline interaction, and a sampling-based approach was employed to consider the uncertainty of soil parameters. This paper uses the same buried gas pipeline structure to derive fragility curves. Yoon et al. [56] selected API 5L X65, a commonly used material for buried gas pipelines in South Korea, for their study, and the material properties are detailed in Table 6. The pipeline has a hollow circular steel section with outer and inner diameters of 762 mm and 727 mm, respectively, and is made of rough steel. For the structural analysis, a straight pipeline measuring 1.2 km in length and 1.881 m from the ground to the pipe cross-section centerline was employed, with the assumption that both ends of the pipeline were fixed. Several reasonable assumptions were applied to the numerical modeling of buried gas pipelines, the details are found in

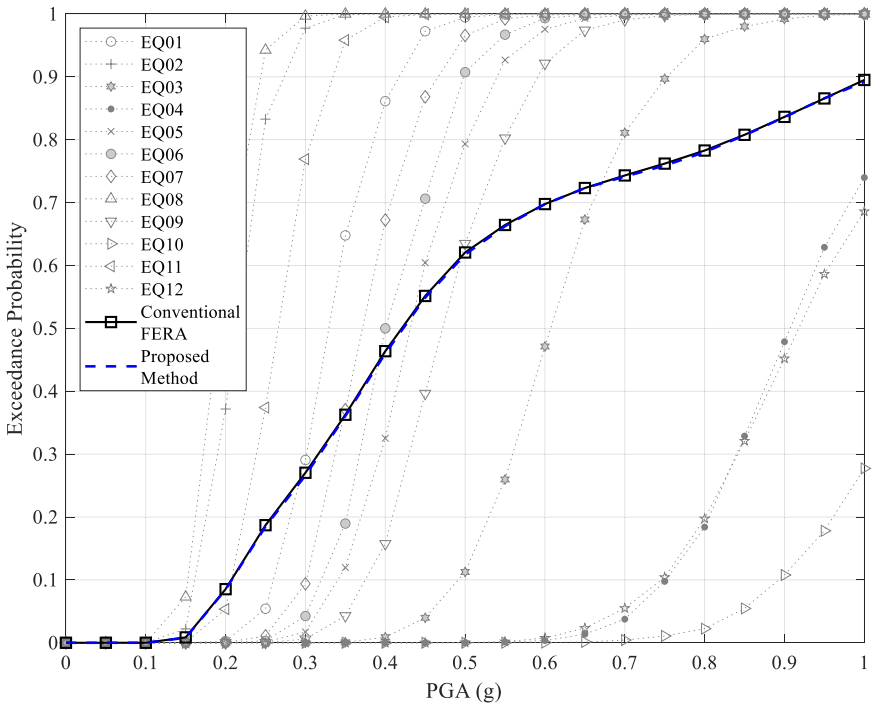

(a) Moderate damage

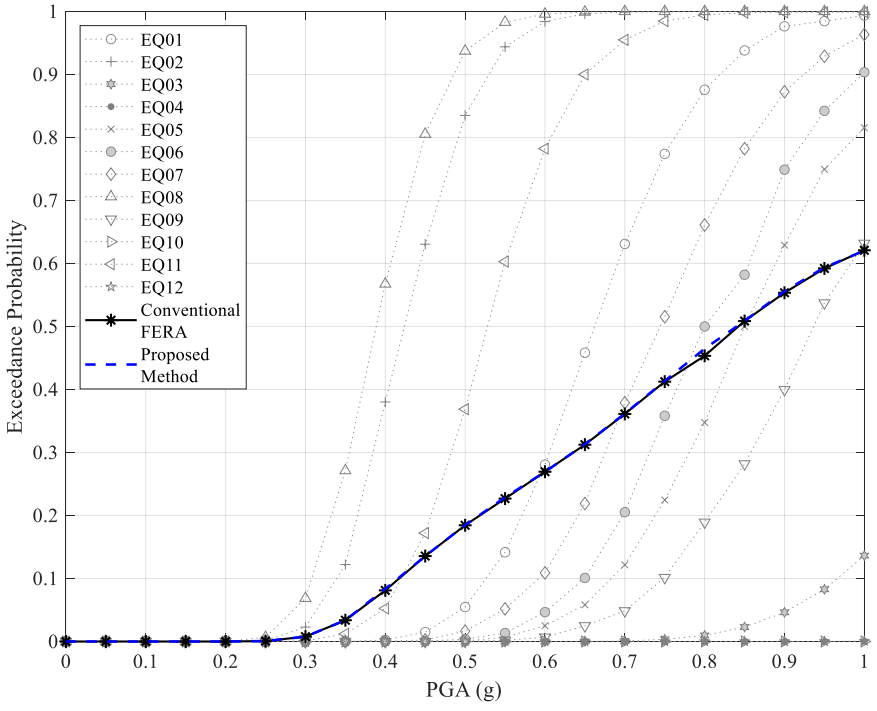

(b) Major damage

Fig. 8. Comparison of seismic fragilities of the conventional FERA and proposed method according to damage states.

[56].

The seismic analysis of the soil-pipeline system was performed using the commercial software ABAQUS, which has a structural model that captures the nonlinear behavior of the buried gas pipeline and its interaction with the surrounding soil. This model employs a constitutive framework to define the soil's stiffness, thus obviating the need for FE discretization. The soil-structure interaction is effectively characterized by the 3D pipe-soil interaction element, PSI34, which simulates the complex nonlinear relationship between the pipeline and the soil region. This allows for a detailed representation of the constitutive response, as described in [58], enhancing the understanding of the pipeline's behavior under seismic conditions. For the numerical simulation, 1000

Table 10
Comparison of the computational cost of the conventional FERA and proposed method according to damage states and ground motions.

	Moderate damage			Major damage		
	Conventional FERA	Proposed Method	Efficiency	Conventional FERA	Proposed Method	Efficiency
EQ01	282	181	35.82 %	923	536	41.93 %
EQ02	181	137	24.31 %	579	394	31.95 %
EQ03	479	297	38.00 %	1184	343	71.03 %
EQ04	615	323	47.48 %	1337	259	80.63 %
EQ05	389	234	39.85 %	798	465	41.73 %
EQ06	383	241	37.08 %	863	489	43.34 %
EQ07	331	186	43.81 %	930	451	51.51 %
EQ08	168	108	35.71 %	459	233	49.24 %
EQ09	425	275	35.29 %	985	345	64.97 %
EQ10	691	311	54.99 %	1281	537	58.08 %
EQ11	232	161	30.60 %	634	476	24.92 %
EQ12	576	311	46.01 %	1259	318	74.74 %
Total	4752	2765	41.81 %	11,232	4846	56.86 %

pipe elements (PIPE31) and PSI34 elements were used to represent gas pipeline and soil domain, respectively. The damping ratio of the system was presumed to be 5 % of the critical damping, applying the Rayleigh damping model. Fig. 7 illustrates the ABAQUS model of the buried gas pipeline, and it demonstrates the strain distribution pattern observed during a crucial time step when subjected to earthquake loading. The maximum strain was observed near the fixed end, and it gradually decreased as the distance from the fixed end increased. Further details on the FE model and its dynamic characteristics are available in [56].

In this application example, the input ground motion sets considering various earthquake wave characteristics are selected [59]. Table 7 lists 12 input ground motions in the axial, transverse, and vertical directions. This paper considers the PGA as an IM to derive the fragility curve, and nonlinear time history analysis is performed on ground motions selected from 0.05 to 1.00 PGA at 0.05 intervals. This analysis accounts for uncertainties not only in seismic ground motion, but also in material properties, including the yield strength of steel (σ_y), and soil parameters. The uncertainty of soil conditions is defined by three parameters that control soil stiffness in the BNWF model: (1) internal friction angle (φ), (2) cohesion (c), and (3) unit weight (γ), which are considered as RVs. These RVs considered in this example were extensively investigated based on several references [56,60,61], and their statistical characteristics are summarized in Table 8.

This paper employs the definitions of damage state suggested by Shinozuka et al. [62] to estimate a seismic fragility curve for a buried gas pipeline. The criteria for these proposed damage states are based on the peak strain observed in the pipeline, determined through seismic risk assessment of underground pipeline networks. The damage states are described as minor, moderate, or major, corresponding to minor leakage, partial leakage, and complete rupture, respectively. Table 9 illustrates the damage states evaluated in this study for the buried gas pipeline, where ε_p denotes the maximum strain during seismic events, and ε_y represents the yield strain of the pipeline.

5.2. Analysis result: seismic fragility curves

A fragility analysis of the buried gas pipeline for various ground motions is performed for comparison between the proposed method and conventional FERA, and the derived fragility curves are exhibited in Fig. 8, using the strain criteria detailed in Table 9. Owing to the absence of the minimum strain for the minor state in Table 9, fragility curves are constructed only for the moderate and major damage states, as shown in Fig. 8. The derived fragility curve gradually increases as the PGA increases. In this paper, 12 ground motions are considered, and the fragility curves derived using the proposed method are depicted in Fig. 8. Furthermore, the average of 12 fragility curves is used for the estimation, and it is nearly identical to the curve derived from the conventional FERA.

Table 10 presents the number of FEAs and efficiency of the proposed method for each damage state and ground motion. For moderate damage, the most efficient ground motion is EQ10, which improves the efficiency of the computational cost by approximately 54.99 % compared with the conventional FERA. In comparison, a relatively less efficient case is EQ2, which has a relatively low efficiency, representing an improvement of approximately 24.31 % compared with the conventional method. EQ4 is the most cost-effective case for major damage and exhibits a computational efficiency of approximately 80.63 % compared with the conventional method. However, a relatively less efficient case is EQ11, which improves the computational cost by approximately 24.92 %, similar to the moderate damage case. In addition, compared with the conventional FERA, the computational cost to derive the fragility curve for moderate damage using the proposed method improves by approximately 41.81 % and by approximately 56.86 % to derive a fragility curve for major damage. This clearly demonstrates that the proposed method can effectively estimate accurate seismic fragility curves with enhanced efficiency.

6. Conclusion

This study introduces a novel approach for efficiently deriving fragility curves through a sequentially-updated surrogate model, significantly improving the computational cost associated with finite element reliability analysis (FERA). The key findings of our research are summarized as follows:

- The proposed method utilizes a sequentially-updated surrogate model to minimize computational demands. This model significantly reduces the number of finite element analyses required within the first-order reliability method (FORM) analysis loop of FERA.
- The surrogate model, constructed using Gaussian process regression (GPR), leverages existing FERA results, thus eliminating the need for additional computational expenses in surrogate modeling process. This approach not only enhances efficiency but also maintains the accuracy of the conventional methods.
- The validity of the proposed method is confirmed through comparative analyses using conventional FERA and Monte Carlo simulations (MCS). Application examples, including a hypothetical short column under biaxial bending and axial load, a bridge subjected to flood fragility analysis considering scour, and a seismic analysis of a buried gas pipeline with soil-structure interactions, demonstrate that the derived fragility curves closely align with those obtained from conventional FERA.
- Documented reductions in computational costs are 36.54 % for the bridge flood fragility analysis and 52.38 % for the seismic fragility analysis of the buried gas pipeline, compared to conventional FERA

methods. These results highlight the method's significant improvement in cost efficiency.

The proposed approach can be extended and applied not only to deriving fragility curves but also to problems such as reliability-based optimization, which requires multiple FERA iterations.

CRediT authorship contribution statement

Jaebeom Lee: Conceptualization, Formal analysis, Methodology, Software, Writing – review & editing. **Seungjun Lee:** Conceptualization, Data curation, Formal analysis, Methodology, Software, Validation, Visualization, Writing – original draft, Writing – review & editing. **Young-Joo Lee:** Conceptualization, Funding acquisition, Investigation, Methodology, Project administration, Resources, Software, Supervision, Writing – original draft, Writing – review & editing. **Sungsik Yoon:** Conceptualization, Formal analysis, Methodology, Software, Writing – review & editing.

Declaration of Competing Interest

The authors declare that they have no known competing financial interests or personal relationships that could have appeared to influence the work reported in this paper.

Acknowledgement

This work was supported by the National Research Foundation of Korea (NRF) grant funded by the Korea government (MSIT) (No. RS-2022-00144434).

References

[1] Ward PJ, Blauhut V, Bloemendaal N, Daniell JE, De Ruiter MC, Duncan MJ, et al. Review article: natural hazard risk assessments at the global scale. Nat Hazards Earth Syst Sci 2020;20:1069–96. https://doi.org/10.5194/nhess-20-1069-2020.
[2] UNISDR U. Sendai framework for disaster risk reduction 2015–2030. In: Proceedings of the third United Nations world conference on DRR. Sendai, Japan; 2015.
[3] FEMA. Hazus—MH 2.1: Technical manual. Multi-hazard loss estimation methodology, earthquake model. Washington, D.C.:FEMA; 2013
[4] NCSA. ERGO-EQ platform for multi-hazard assessment response and planning. National Center for Supercomputing Applications and Mid America Earthquake Center; 2024. Available from: http://ergo.ncsa.illinois.edu/. [Accessed 1 January 2024].
[5] Pitilakis K, Franchin P, Khazai B, Wenzel H. Systemic seismic vulnerability and risk assessment of complex urban, utility, lifeline systems and critical facilities: methodology and applications. Dordrecht: Springer; 2014. https://doi.org/10.1007/978-94-017-8835-9.
[6] Silva V, Crowley H, Pagani M, Monelli D, Pinho R. Development of the OpenQuake engine, thE Global Earthquake Model's open-source software for seismic risk assessment. Nat Hazards 2014;72:1409–27. https://doi.org/10.1007/s11069-013-0618-x.
[7] Decò A, Frangopol DM. Risk assessment of highway bridges under multiple hazards. J Risk Res 2011;14:1057–89. https://doi.org/10.1080/13669877.2011.571789.
[8] Silva V, Crowley H, Varum H, Pinho R, Sousa R. Evaluation of analytical methodologies used to derive vulnerability functions. Earthq Eng Struct Dyn 2014;43:181–204. https://doi.org/10.1002/eqe.2337.
[9] Zentner I, Gündel M, Bonfils N. Fragility analysis methods: review of existing approaches and application. Nucl Eng Des 2017;323:245–58. https://doi.org/10.1016/j.nucengdes.2016.12.021.
[10] Kiani J, Camp C, Pezeshk S. On the application of machine learning techniques to derive seismic fragility curves. Comput Struct 2019;218:108–22. https://doi.org/10.1016/j.compstruc.2019.03.004.
[11] Padgett JE, Nielson BG, DesRoches R. Selection of optimal intensity measures in probabilistic seismic demand models of highway bridge portfolios. Earthq Eng Struct Dyn 2008;37:711–25. https://doi.org/10.1002/eqe.782.
[12] NIWA. RiskScape: Flood fragility methodology - NIWA technical report: WLG2010–45. New Zealand; New Zealand Climate Change Research Institute; 2011
[13] Rossetto T, Elnashai A. Derivation of vulnerability functions for European-type RC structures based on observational data. Eng Struct 2003;25:1241–63. https://doi.org/10.1016/S0141-0296(03)00060-9.
[14] Nofal OM, van de Lindt JW, Do TQ. Multi-variate and single-variable flood fragility and loss approaches for buildings. Reliab Eng Syst Saf 2020;202:106971. https://doi.org/10.1016/j.ress.2020.106971.
[15] Rosti A, Rota M, Penna A. Empirical fragility curves for Italian URM buildings. Bull Earthq Eng 2020;19:3057–76. https://doi.org/10.1007/s10518-020-00845-9.
[16] Van De Lindt JW, Peacock WG, Mitrani-Reiser J, Rosenheim N, Deniz D, Dillard M, et al. Community resilience-focused technical investigation of the 2016 Lumberton, North Carolina, flood: an interdisciplinary approach. Nat Hazards Rev 2020;21:04020029. https://doi.org/10.1061/(ASCE)NH.1527-6996.0000387.
[17] Kwon O-S, Elnashai A. The effect of material and ground motion uncertainty on the seismic vulnerability curves of RC structure. Eng Struct 2006;28:289–303. https://doi.org/10.1016/j.engstruct.2005.07.010.
[18] Dong Y, Frangopol DM. Probabilistic life-cycle cost-benefit analysis of portfolios of buildings under flood hazard. Eng Struct 2017;142:290–9. https://doi.org/10.1016/j.engstruct.2017.03.063.
[19] Lee S, Moon D-S, Kim B, Kim J, Lee Y-J. Hybrid fragility curve derivation of buildings based on post-earthquake reconnaissance data. Smart Struct Syst 2021;28:553–66. https://doi.org/10.12989/sss.2021.28.4.553.
[20] Kwon O.-S. Probabilistic seismic assessment of structure, foundation, and soil interacting systems [Ph.D. dissertation]. IL, USA: University of Illinois, Urbana; 2007.
[21] Lee Y-J, Moon D-S. A new methodology of the development of seismic fragility curves. Smart Struct Syst 2014;14(5):847–67. https://doi.org/10.12989/sss.2014.14.5.847.
[22] Soleimani F, Hajializadeh D. State-of-the-art review on probabilistic seismic demand models of bridges: machine-learning application. Infrastructures 2022;7(5):64. https://doi.org/10.3390/infrastructures7050064.
[23] Kudela J, Matousek R. Recent advances and applications of surrogate models for finite element method computations: a review. Soft Comput 2022;26:13709–33. https://doi.org/10.1007/s00500-022-07362-8.
[24] Ghosh J, Padgett JE, Dueñas-Osorio L. Surrogate modeling and failure surface visualization for efficient seismic vulnerability assessment of highway bridges. Probab Eng Mech 2013;34:189–99. https://doi.org/10.1016/j.probengmech.2013.09.003.
[25] Zhang Y, Wu G. Seismic vulnerability analysis of RC bridges based on Kriging model. J Earthq Eng 2019;23(2):242–60. https://doi.org/10.1080/13632469.2017.1323040.
[26] Kim T, Song J, Kwon O-S. Probabilistic evaluation of seismic responses using deep learning method. Struct Saf 2020;84:101913. https://doi.org/10.1016/j.strusafe.2019.101913.
[27] Khandel O, Soliman M. Integrated framework for assessment of time-variant flood fragility of bridges using deep learning neural networks. J Infrastruct Syst 2021;27(1):04020045. https://doi.org/10.1061/(ASCE)IS.1943-555X.0000587.
[28] Kameshwar S, Padgett JE. Multi-hazard risk assessment of highway bridges subjected to earthquake and hurricane hazards. Eng Struct 2014;78:154–66. https://doi.org/10.1016/j.engstruct.2014.05.016.
[29] Seo J, Pokhrel J, Hu JW. Multi-hazard fragility analysis of offshore wind turbine portfolios using surrogate models. Renew Sustain Energy Rev 2022;165:112552. https://doi.org/10.1016/j.rser.2022.112552.
[30] Samadian D, Muhit IB, Occhipinti A, Dawood N. Meta databases of steel frame buildings for surrogate modelling and machine learning-based feature importance analysis. Resil Cities Struct 2024;3(1):20–43. https://doi.org/10.1016/j.rcns.2023.12.001.
[31] Alizadeh R, Allen JK, Mistree F. Managing computational complexity using surrogate models: a critical review. Res Eng Des 2020;31:275–98. https://doi.org/10.1007/s00163-020-00336-7.
[32] Melchers RE, Beck AT. Structural reliability analysis and prediction. John Wiley & Sons Ltd; 2018.
[33] Rackwitz R, Flessler B. Structural reliability under combined random load sequences. Comput Struct 1978;9(5):489–94. https://doi.org/10.1016/0045-7949(78)90046-9.
[34] Der Kiureghian A. First- and second-order reliability methods. In: Nikolaidis E, Ghiocel DM, Singhal S, editors. Engineering design reliability handbook. CRC Press; 2005.
[35] Lee Y.-J., Song J., Tuegel E. Finite element system reliability analysis of a wing torque box. In: Proceedings of the tenth AIAA nondeterministic approaches conference, Schaumburg, IL, April; 2008. Available from: https://doi.org/10.2514/6.2008–1718.
[36] Lee J, Lee Y-J, Kim H, Sim S-H, Kim J-M. A new methodology development for flood fragility curve derivation considering structural deterioration for bridges. Smart Struct Syst 2016;17(1):149–65. https://doi.org/10.12989/sss.2016.17.1.149.
[37] Haukaas T. Finite element reliability and sensitivity methods for performance-based engineering [Ph.D. dissertation]. Berkeley, CA, USA: University of California; 2003.
[38] Afshari SS, Enayatollahi F, Xu X, Liang X. Machine learning-based methods in structural reliability analysis: a review. Reliab Eng Syst Saf 2022;219:108223. https://doi.org/10.1016/j.ress.2021.108223.
[39] Stefanou G. The stochastic finite element method: past, present and future. Comput Methods Appl Mech Eng 2009;198(9-12):1031–51. https://doi.org/10.1016/j.cma.2008.11.007.
[40] Khuri AI, Mukhopadhyay S. Response surface methodology. Wiley Interdiscip Rev Comput Stat 2010;2(2):128–49. https://doi.org/10.1002/wics.73.
[41] Chojaczyk AA, Teixeira AP, Neves LC, Cardoso JB, Soares CG. Review and application of artificial neural networks models in reliability analysis of steel

structures. Struct Saf 2015;52:78–89. https://doi.org/10.1016/j.strusafe.2014.09.002.
[42] Roy A, Chakraborty S. Support vector machine in structural reliability analysis: a review. Reliab Eng Syst Saf 2023;233:109126. https://doi.org/10.1016/j.ress.2023.109126.
[43] Kaymaz I. Application of kriging method to structural reliability problems. Struct Saf 2005;27(2):133–51. https://doi.org/10.1016/j.strusafe.2004.09.001.
[44] Gaspar B, Teixeira AP, Soares CG. Assessment of the efficiency of Kriging surrogate models for structural reliability analysis. Probabilistic Eng Mech 2014;37:24–34. https://doi.org/10.1016/j.probengmech.2014.03.011.
[45] Lataniotis C, Marelli S, Sudret B. The Gaussian process modeling module in UQLab. J Soft Comput Civ Eng 2018;2(3):91–116. https://doi.org/10.22115/SCCE.2018.129323.1062.
[46] Barber D. Bayesian reasoning and machine learning. Cambridge University Press; 2012.
[47] Rasmussen CE, Williams CKI. Gaussian processes for machine learning. MIT Press; 2006.
[48] Liu PL, Der Kiureghian A. Multivariate distribution models with prescribed marginals and covariances. Probab Eng Mech 1986;1(2):105–12. https://doi.org/10.1016/0266-8920(86)90033-0.
[49] Korea Road & Transportation Association. Korean highway bridge design specification (KHBDS). Seoul: Ministry of Land, Transport and Maritime Affairs of Korea. (in Korean); 2010.
[50] Kim H, Sim S-H, Lee J, Lee Y-J, Kim J-M. Flood fragility analysis for bridges with multiple failure modes. 1687814017696415 Adv Mech Eng 2017;9(3). https://doi.org/10.1177/1687814017696415.
[51] Lehký D., Keršner Z., Novák D. Determination of statistical material parameters of concrete using fracture test and inverse analysis based on FraMePID-3PB tool. In: Proceedings of the fifth international conference on reliable engineering computing, Brno, Czech Republic; June 2012.
[52] Ju M, Oh H, Sun J-W. Simplified reliability estimation for optimum strengthening ratio of 30-year-old double T-beam railway bridge by NSM techniques. Math Probl Eng 2014:734016.
[53] Song S.T., Chai Y.H., Hale T.H. Limit state analysis of fixed-head concrete piles under lateral loads. In: Proceedings of the thirteenth world conference on earthquake engineering, Vancouver, BC, Canada; August 2004.
[54] Chiou J-S, Chiang C-H, Yang H-H, Hsu S-Y. Developing fragility curves for a pile-supported wharf. Soil Dyn Earthq Eng 2011;31(5-6):830–40. https://doi.org/10.1016/j.soildyn.2011.01.011.
[55] Caltrans. Seismic design criteria, California DOT: Sacramento, California; 2006.
[56] Yoon S, Lee DH, Jung H-J. Seismic fragility analysis of a buried pipeline structure considering uncertainty of soil parameters. Int J Press Vessel Pip 2019;175:103932. https://doi.org/10.1016/j.ijpvp.2019.103932.
[57] Yankelevsky DZ, Eisenberger M, Adin MA. Analysis of beams on nonlinear winkler foundation. Comput Struct 1989;31(2):287–92. https://doi.org/10.1016/0045-7949(89)90232-0.
[58] Audibert JM, Nyman DJ, O'Rourke TD. Differential ground movement effects on buried pipelines. Guidel Seism Des Oil Gas Pipeline Syst 1984:150–83.
[59] Lee DH, Kim BH, Jeong S-H, Jeon J-S, Lee T-H. Seismic fragility analysis of a buried gas pipeline based on nonlinear time-history analysis. Int J Steel Struct 2016;16:231–42. https://doi.org/10.1007/s13296-016-3017-9.
[60] Jones A.L., Kramer S.L., Arduino P. Estimation of uncertainty in geotechnical properties for performance-based earthquake engineering, PEER report 2002–16. Berkeley, CA: Pacific Earthquake Engineering Research Center, University of California; 2002.
[61] Keshtegar B, Miri M. Reliability analysis of corroded pipes using conjugate HL–RF algorithm based on average shear stress yield criterion. Eng Fail Anal 2014;46:104–17. https://doi.org/10.1016/j.engfailanal.2014.08.005.
[62] Shinozuka M, Takada S, Ishikawa H. Some aspects of seismic risk analysis of underground lifeline systems. J Press Vessel Technol 1979;101(1):31–43. https://doi.org/10.1115/1.3454596.